CFD Analysis of Biomass Gasification Using Bubbling Fluidized Bed Gasification Technique

Jay J. Makwana[1], Umang J. Patadiwala[2], Dharmendra Sapariya[3]

[1]Student, Department of Mechanical Engineering, M. Tech (CAD/CAM), INDUS University, Ahmedabad, Gujarat, India.
[2]Professor, Department of Mechanical Engineering, INDUS University, Ahmedabad, Gujarat, India.
[3]Professor, Department of Mechanical Engineering, INDUS University, Ahmedabad, Gujarat, India.

Abstract: The bubbling fluidized bed gasifier is the one most important technology of the gasification through which biomass fuel like Municipal Solid Waste (MSW) is incompletely burnt in the presence of air and then converted into high calorific value gases fuel. The capabilities of bubbling fluidized bed gasifier are affected by feedstocks characteristics, process parameters and design parameters. CFD simulation have been done for improvement of process parameters for Municipal Solid Waste and Sugarcane Bagasse. CFD simulations are carried for a cylinder-shaped bubbling fluidized bed with a static bed height of 0.665m with 0.144m diameter of rector chamber and 1.46m reactor height. The gas-solid hydrodynamics and gasification process inside a fluidized-bed biomass gasifier are calculated using the CFD solver ANSYS-FLUENT 20.0. A 2-D rectangular model based on Eulerian-Eulerian approach attached with granular kinetic theory has been established to simulate the bed hydrodynamics for the BFBG where volume fraction, bed pressure drops and velocities has been focused using ANSYS Fluent software. The effects of particle properties, gas velocity and temperature of bed material within the reactor has been examined approximately for simulation which provides a significant basis for detailed design of BFBG.

Keywords: **Bubbling Fluidized Bed, Gasification, Municipal Solid Waste, Sugarcane Bagasse Syngas, CFD, ANSYS/*FLUENT***

I. INTRODUCTION

The bubbling fluidized bed gasifier is more efficient technology through which the gasification process takes place. In fluidization process, the grinding or small particles reacts as fluid when it is pass through moving fluid. Design parameters such as biomass feeding systems, air supply systems and ash removal systems also affect the performance of bubbling gasifiers. To increasing the mixing rate of air and fuel also affected the performance of the gasifier by using perforated plate distributors. The biomass like Municipal Solid Waste (MSW) is one of the renewable energy sources, which helps in power generation. India is the 7th largest country in the world covering 328 million hectares and is adequately equipped with renewable energy sources. Among renewable energy sources, biomass plays a major role especially in rural areas, as it is a major source of energy for many Indian households. Biomass can be used as a source of energy through thermal or biological conversion channels into a range of useful energy products such as heat, electricity, hydrogen, liquid fuels and fusion gas.

II. DESIGN OF BUBBLING FLUIDIZED BED GASIFIER

The gasifier design was derived from various literatures and the reference books. The model was developed separately for each velocity parameters. (Kunii, D., Levenspiel, O., & Levenspiel, O. 1990, Ifin, N. E. 2001)

Design Parameters	Equations	Sand	MSW	Bagasse
Minimum fluidization velocity U_{mf}	$U_{mf} = \frac{d_p^2(\rho_s - \rho_g)g}{150 * \mu} * \frac{\varepsilon^3 * \phi^2}{1-\varepsilon}$	0.073 (m/s)	0.17 (m/s)	0.083 (m/s)
Terminal Velocity U_t	$U_t = d_p \left[\frac{4(\rho_p - \rho_g)^2 g^2}{225 * \rho_g * \mu}\right]^{1/3}$	3.22 (m/s)	2.41 (m/s)	2 (m/s)
Fluidization Velocity U_{mf}	$\frac{H}{H_{mf}} = 1 + \frac{10.978(U_f - U_{mf})^{0.738}\rho_p^{0.376}d_p^{1.006}}{U_{mf}^{0.937}\rho_g^{0.126}}$	0.48 (m/s)	0.63 (m/s)	0.50 (m/s)
Characterizing the fluidization in the reactor	$u^* = u\left[\frac{\rho_g^2}{\mu * (\rho_p - \rho_g) * g}\right] d^* = d_p\left[\frac{\rho_g(\rho_p - \rho_g)g}{\mu^2}\right]^{1/3}$	0.16 6.70	1.13 14.77	0.35 7.85
Slugging Velocity U_{s1} Max Bed Height H_{fb} Bed Height for Stable Slugging Z_s	$U_{s1} = U_{mf} + 0.07(gD)^{0.5}$ $H_{fb} = \frac{D - 2.51 * D^{0.2}}{0.13 * D^{0.47}}$ $Z_s = 60 * D^{0.175}$	15.63(mm/s) 22.23 (cm) 95.69 (cm)	16.65(mm/s) 22.23(cm) 95.69(cm)	25.70(mm/s) 22.23(cm) 95.69(cm)
Bed Height	$L_{mf} = \frac{L}{1 + \frac{10.978(U_f - U_{mf})^{0.738}\rho_p^{0.376}d_p^{1.006}}{U_{mf}^{0.937}\rho_g^{0.126}}}$	14.60(cm)	14.96(cm)	14.70(cm)
Reactor Diameter	$F_{car,I} = 6.0 * 10^{-7} * S * P$	14.4(cm)	14.4(cm)	14.4(cm)
Reactor Height	$L = \tau * \frac{Q}{\left(\frac{\pi}{4}\right) * d^2}$	1.44 (m)	1.44 (m)	1.44 (m)

Table 1. Fluidization Calculation

Combustion Calculation for MSW and Bagasse

Ultimate analysis (wt. %)						
Biomass	C	H	O	N	S	Empirical Formula
MSW	35.1	4.7	16.1	1.4	0.2	$CH_{1.606}O_{0.343}N_{0.3418}$ $S_{0.0021}$
Bagasse	59.335	6.259	33.750	0.656	0	$CH_{0.633}$ $O_{0.213}$ $N_{0.005}$
Proximate analysis (wt. %)						
Biomass	MC	VM	FC	ASH		HHV (MJ/kg)
MSW	45.8	51.1	6.3	42.6		15.3
Bagasse	9.577	72.181	14.341	3.9		24.47

Table 2. Ultimate and Proximate analysis of MSW

Material	Airflow Rate (kg/hr)	Biomass Flow Rate(kg/hr)
MSW	13 to 15	10
Bagasse	13 to 15	10

Table 3. Mass Flowrate of Biomass and Air

The distributor plate sits at the bottom of the reactor, it allows for the gasses to enter the reactor and fluidize the bed as well as provide support for the bed inside the reactor. The Primary function of the distributor plate is to distribute the fluidizing gas uniformly for the design of the fluidized bed a perforated distributor plate was chosen for ease and convenience.

Design Criteria for Distributor Plate	
Number of Orifice (m^2)	32
Diameter of Orifice (mm)	2
Triangular Pitch (mm)	26

Table 4. Distributor Plate Design

The cyclone was designed using the Lapple method, as outlined in Air Pollution Control, A Design Approach. The Lapple method determined the optimum dimensions for different types of cyclones in relation to the body diameter of the cyclone so the results can be applied for general use.

Cyclone Separator Design	in mm
Diameter of Cyclone Shell (Dc)	147
Outlet Pipe Diameter (De)	40
Height of Inlet Pipe (Hc)	76.5
Width of Inlet Pipe (Bc)	39.75
Length of Cylindrical Shell and Conical Shell (Lc) & (Zc)	295
Vertical Distance of the Outlet pipe from inlet pipe (Sc)	18.375
Diameter of Ash Bin (Jc)	300

Table 5. Cyclone Separator Design Parameters

Property	Sand	MSW	Bagasse
Particle Size (μm)	385	2500	850
Density (kg/m3)	2650	100.62	389
Porosity (ε)	0.46	0.60	0.64
Sphericity (ø)	0.78	0.55	0.49

Table 6. Properties of Sand and MSW

III. COMPUTATIONAL METHOD

ANSYS FLUENT is utilized for simulation wherein 2nd segregated first order implicit unsteady solver is utilized for multiphase calculations. The usage of Eulerian - Eulerian multiphase version, fashionable k-ε dispersed Eulerian multiphase model with standard wall functions are used. Gas is taken as continuous phase while sand particles are taken as dispersed phase. Kinetic theory of granular flow has been applied to sand particles. Syamlal O'Brien drag model of interphase interaction (Solid-Gas) is used. The bed material considered for the analysis is sand, an inert material. Bed fluidizing medium is air.

IV. GOVERNING EQUATIONS

CFD ANSYS Fluent 20.0 Eulerian-Eulerian multiphase model is applied for simulation of a 2D bed containing MSW and Bagasse particles of mean diameter 2.5 mm and 0.85 mm, while the gas moves upwardly in the bed. To predict the bed hydrodynamics, air is considered the primary phase while MSW and Bagasse are considered secondary or discreate phase. The particles are assumed as a continuum phase so kinetic theory of granular flow (KTGF) is applied. The conservation equations for gas and solid phases are given below. (Abd-Rabbo, M. A., Sakr, R. Y., Mohammad, M. A., & Mandour, M. M. 2019)

Volume Fraction	$\varepsilon_g + \varepsilon_s = 1$
Conservation of Mass	Gas: $\frac{\partial(\varepsilon_g \rho_g)}{\partial t} + \nabla.(\varepsilon_g \rho_g \vec{v}_g) = 0$ Solid: $\frac{\partial(\varepsilon_s \rho_s)}{\partial t} + \nabla.(\varepsilon_s \rho_s \vec{v}_s) = 0$
Conservation of Momentum	Gas: $\frac{\partial(\varepsilon_g \rho_g \vec{v}_g)}{\partial t} + \nabla.(\varepsilon_g \rho_g \vec{v}_g \vec{v}_g) = -\varepsilon_g \nabla P + \nabla.\bar{\bar{T}}_g + (\varepsilon_g \rho_g \vec{g}) + K_{gs}(\vec{v}_g - \vec{v}_s)$ Solid: $\frac{\partial(\varepsilon_s \rho_s \vec{v}_s)}{\partial t} + \nabla.(\varepsilon_s \rho_s \vec{v}_s \vec{v}_s) = -\varepsilon_s \nabla P + \nabla.\bar{\bar{T}}_s + (\varepsilon_s \rho_s \vec{g}) + K_{gs}(\vec{v}_g - \vec{v}_s)$
The stress tensors	Gas: $\bar{\bar{T}}_g = \varepsilon_g \mu_g \nabla.\vec{v}_g + \varepsilon_g \mu_g \vec{v}_g{}^T - \frac{2}{3}\varepsilon_g \mu_g \nabla.\vec{v}_g I$ Solid: $\bar{\bar{T}}_s = \varepsilon_s \mu_b \nabla.\vec{v}_s \bar{\bar{I}} + \varepsilon_s \mu_s \nabla \vec{v}_s + \varepsilon_s \mu_s \vec{v}_s{}^T - \frac{2}{3}\varepsilon_s \mu_s \nabla.\vec{v}_s \bar{I}$
Conservation of Energy	Gas: $\frac{\partial(\varepsilon_g \rho_g H_g)}{\partial t} + \nabla.(\varepsilon_g \rho_g \vec{v}_g H_g) = \nabla.\varepsilon_g K_g^{eff} \nabla T_g - h_{gs}(T_s - T_q)$ Solid: $\frac{\partial(\varepsilon_s \rho_s H_s)}{\partial t} + \nabla.(\varepsilon_s \rho_s \vec{v}_s H_s) = \nabla.\varepsilon_s K_s^{eff} \nabla T_s - h_{sg}(T_s - T_g)$
Syamlal O'Brien drag model	$K_{gs} = \frac{3}{4}\frac{\varepsilon_g \rho_g H_g}{v_{t,s}^2 d_s} C_D \left(\frac{Re_s}{v_{r,s}}\right) \lvert \vec{v}_s - \vec{v}_g \rvert$

Table 7. Governing Equations

V. Geometry and Mesh and 3D CAD Model

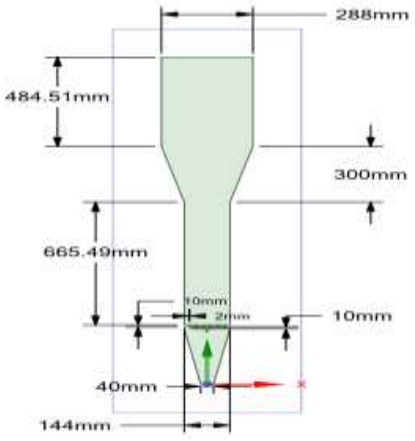

Fig 1. 2D Geometry of BFBG With Dimensions

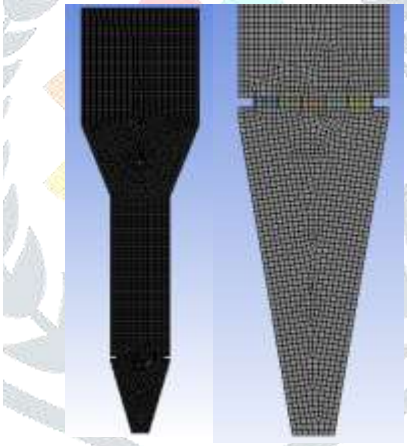

Fig 2. Mesh geometry and Closer View

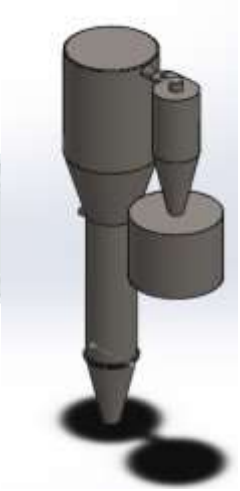

Fig 3. 3D CAD Model of BFBG

Element Size (mm)	5
Number of Elements	13430
Number of Nodes	13880

Table 8. Mesh Details

VI. Solution Procedure

ANSYS FLUENT 20.0 is used to solve the above problems. Phase Couple SIMPLE algorithm is used for Pressure-Velocity communication. The Second Order Implicit scheme is used for non-compliant formats and a fast algorithm is used to classify the words it contains. Each simulation was performed in 2 s and the average time was performed between 0.5 s to 2 s. A small step of 1x10-3 s time is used to avoid instability. 2000 Number of time steps used in simulation.

VII. Results and Discussion

In this study, CFD simulation were performed to validate the hydrodynamics of gas-solid multiphase flow in the bubbling fluidized bed gasifier model. This validation is required for the efficient operation of the control system in this separation process and for the construction of another temperature model. The hydrodynamic behavior of the BFBG was analyzed by monitoring the contour of the solid volume fraction section, the air sand velocity magnitude profile and the pressure profile. The distribution of a fraction of the volume on a bed filled with sand, MSW and Bagasse particles compared to three air velocities, 0.19, 0.22 and 0.30 m / s using the Syamlal and O'Brien drag model is shown in Fig. 3 and 10.

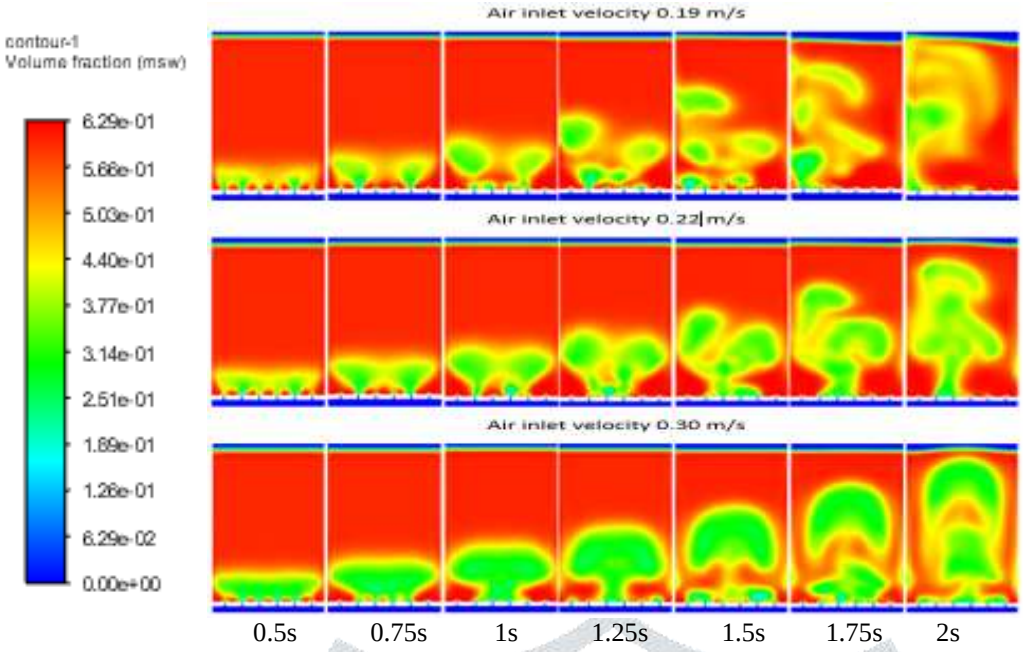

Fig 4. Volume fraction distribution for the MSW particles using the Syamlal and O'Brien drag model with three inlet velocities 0.19 m/s, 0.22 m/s and 0.30 m/s.

It can be seen in Figure 4 which increases the air velocity vs bed height over time. The Void fraction also increases with the increase of the bed in the reactor. The production of small bubbles due to the ingress of air from the bottom of the gasifier is achieved in the early stages of simulation. Bubbles rise up against a wall and grow in an axial direction, either when exiting or meeting small bubbles that form large until they reach the top of the bed. MSW particles are most commonly found in the middle and upper parts of the bed. The movement of the MSW across the bed was centered mainly on the center line of the reactor and below the region near the wall.

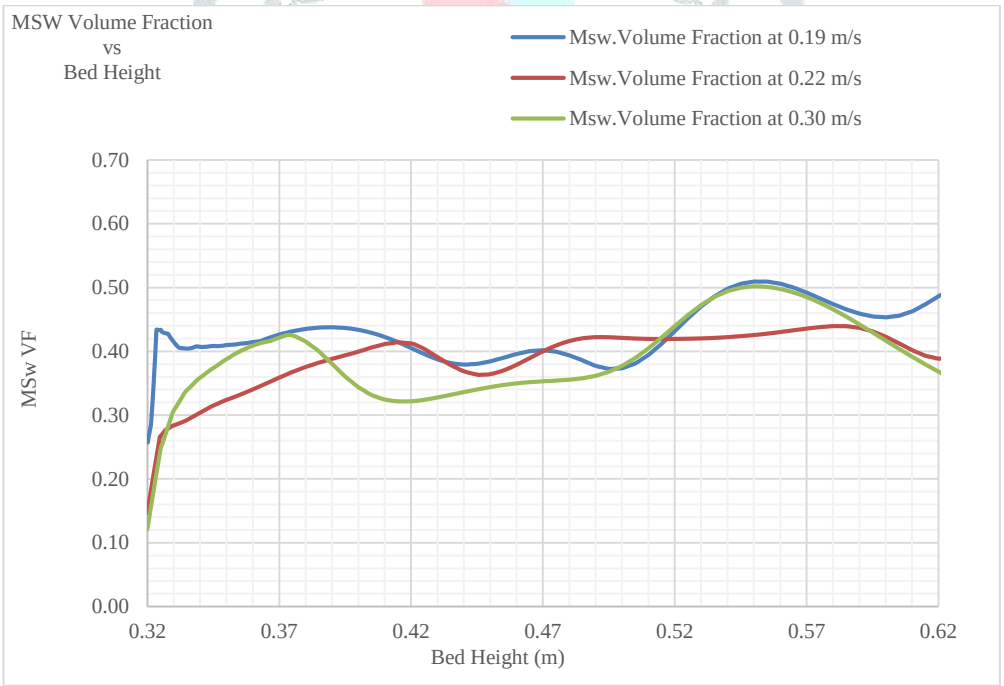

Fig 5. Graph of MSW volume fraction vs Bed Height at Different inlet Air Velocities

Fig 5 shows the simulation results of MSW void fraction vs Bed Height at different air inlet velocities, with increasing air inlet velocity, void fraction also increases. At the start of the simulation, waves of voidage are created, which travel through the bed and subsequently break to form bubbles as the simulation progresses.

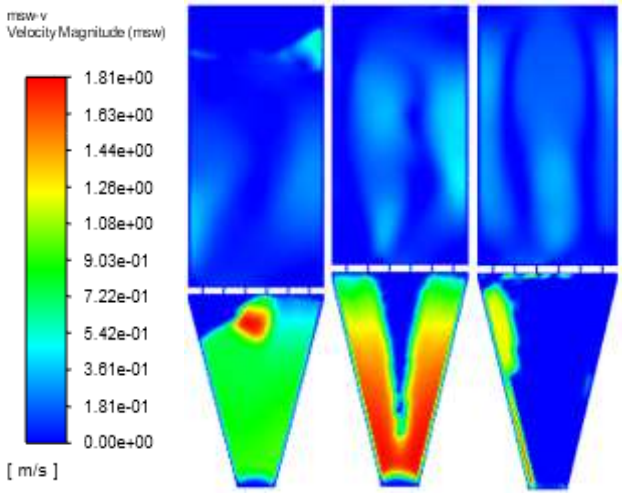

Fig 6. MSW Velocity Magnitude at Different air Inlet Velocities

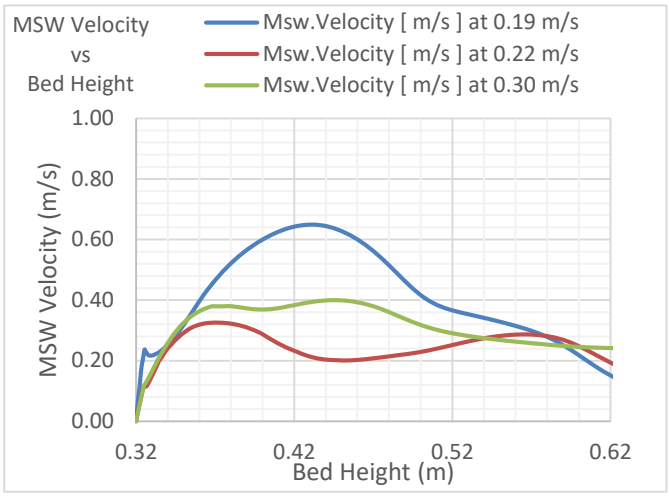

Fig 7. Graph of MSW velocity magnitude vs Bed Height at Different Inlet Air Velocities

Fig 6 shows velocity magnitude of MSW at different air inlet velocities. At low velocities like 0.19 solid particles going downward below distributor plate as the velocity increase solid particles of MSW going upward direction above distributor plate. As shown in Fig 7 at 0.19 m/s air inlet velocity it increases up to 0.65 at middle of bed height comparing to other velocities.

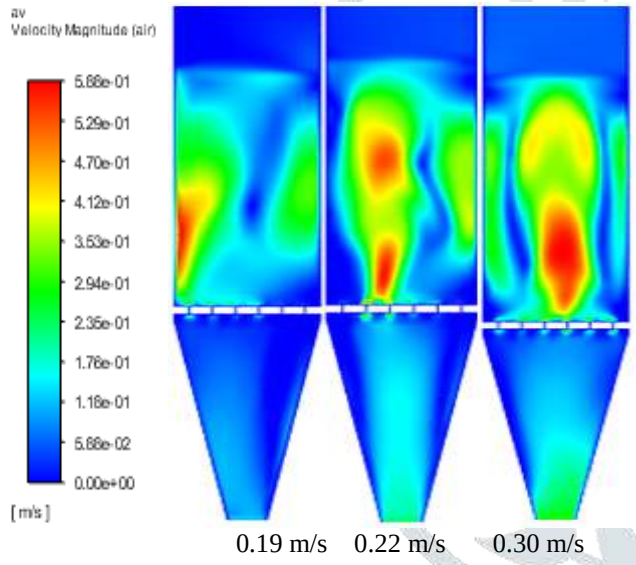

Fig 8. Air Velocity Magnitude at Different air Inlet Velocities

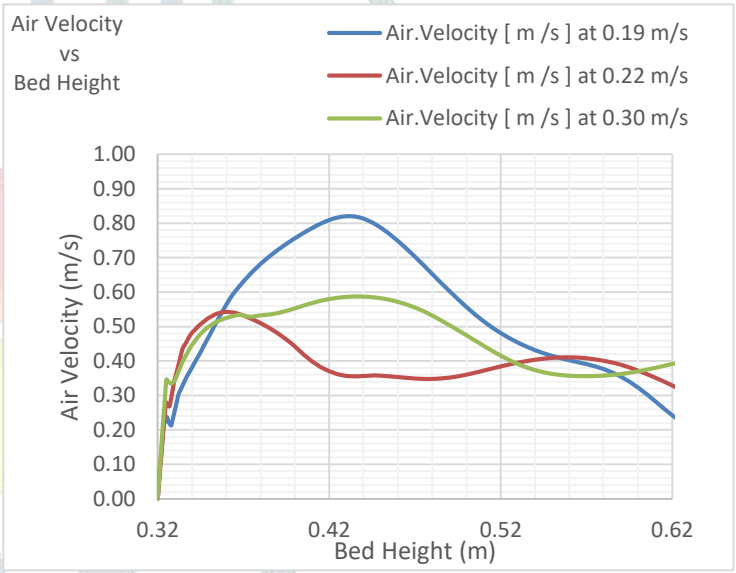

Fig 9. Graph of Air velocity magnitude vs Bed Height at Different Inlet Air Velocities

Fig 8 and 9 shows air inlet velocities in bed height. As increase in velocity it shows various graph plots. At the end of bed height velocity increase between 0.25 to 0.40 m/s.

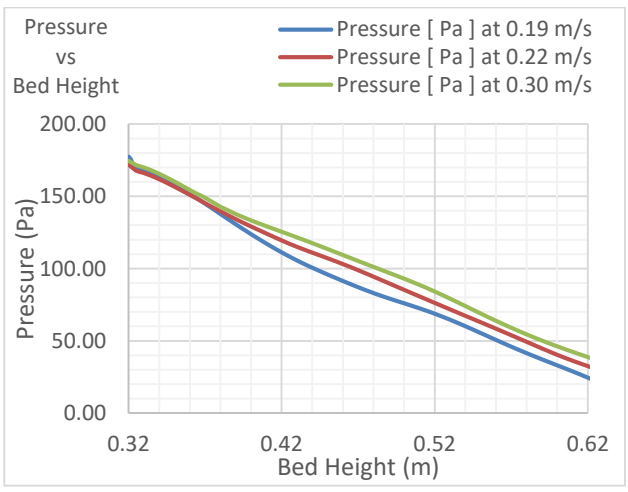

Fig 10. Pressure vs Bed Height at Different inlet Air Velocities

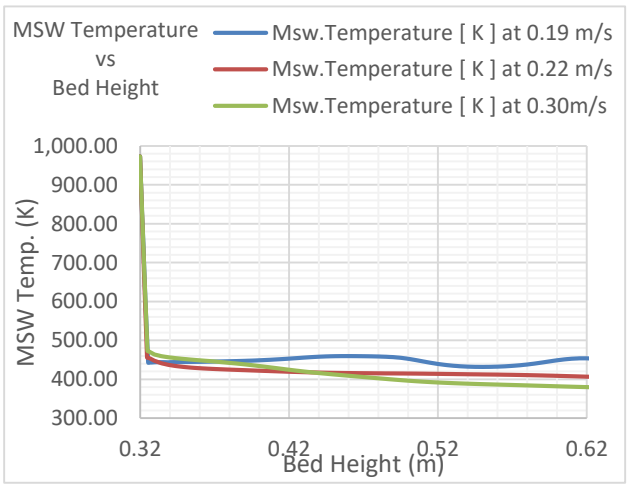

Fig 11. MSW Temperature vs Bed Height at Different inlet Air Velocities

Fig 10 shows pressure of air MSW mixture in bed height. Starting pressure at different air inlet velocities was same. But at the end of bed height, it shows variation between 22 to 40 Pascal. Fig 11 shows Temperature distribution of MSW particles Along the bed. It shows small variation about 390 k to 480 k at different inlet velocities.

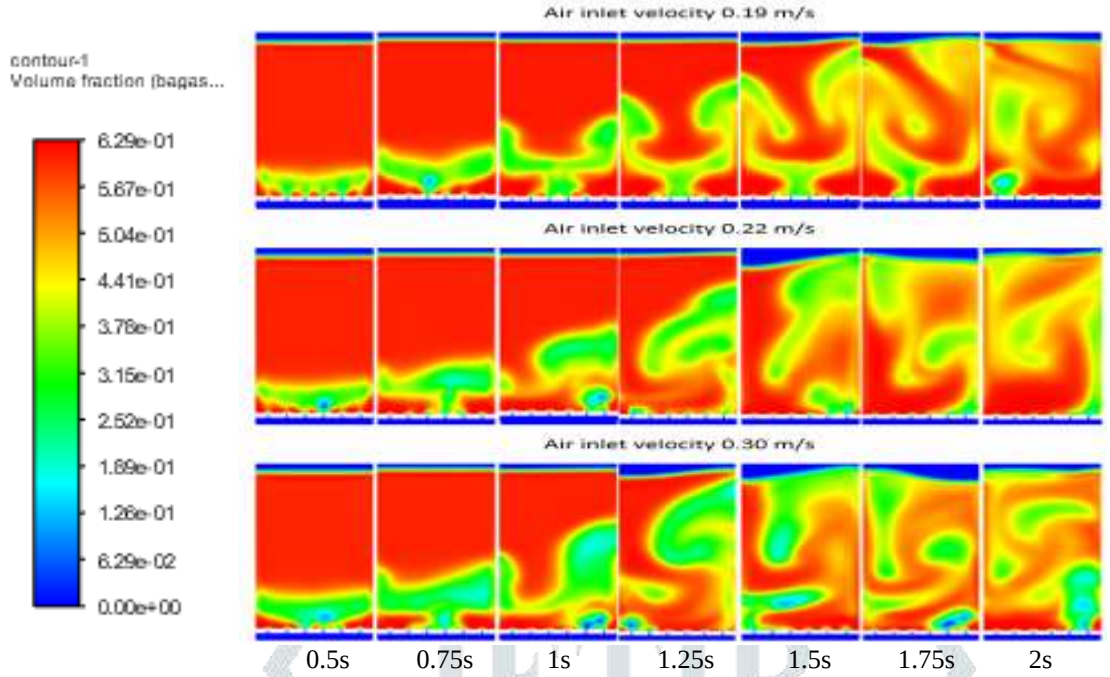

Fig 12. Volume fraction distribution for the Bagasse particles using the Syamlal and O'Brien drag model with three inlet velocities 0.19 m/s, 0.22 m/s and 0.30 m/s.

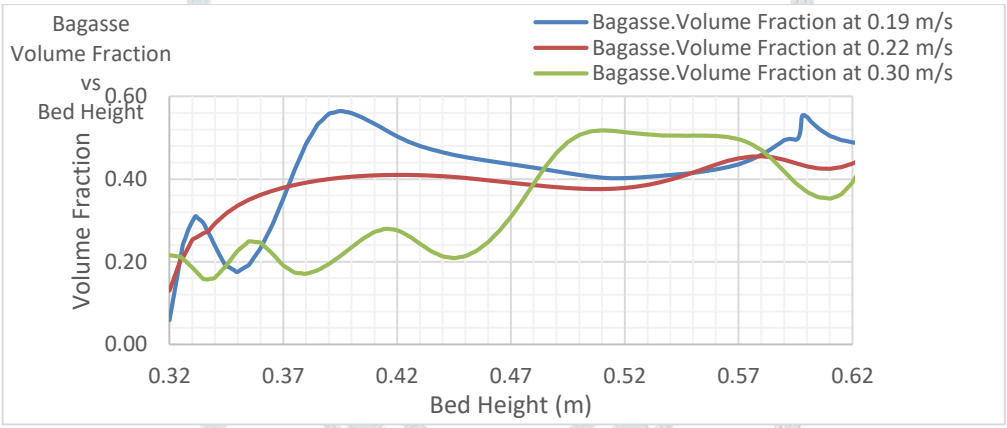

Fig 13. Graph of MSW velocity magnitude vs Bed Height at Different inlet Air Velocities

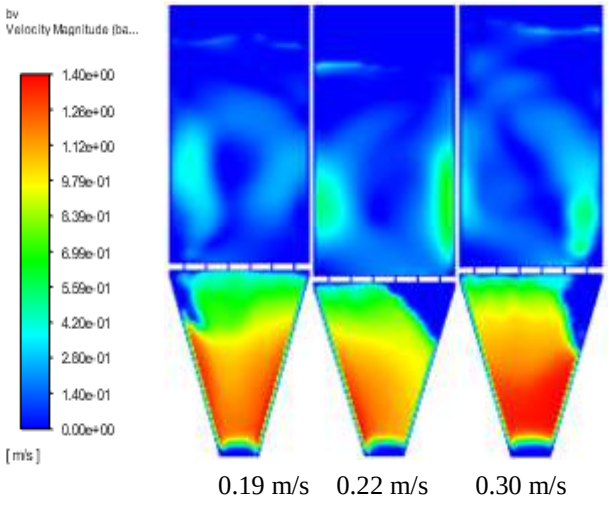

Fig 14. Bagasse Velocity Magnitude at Different air Inlet Velocities

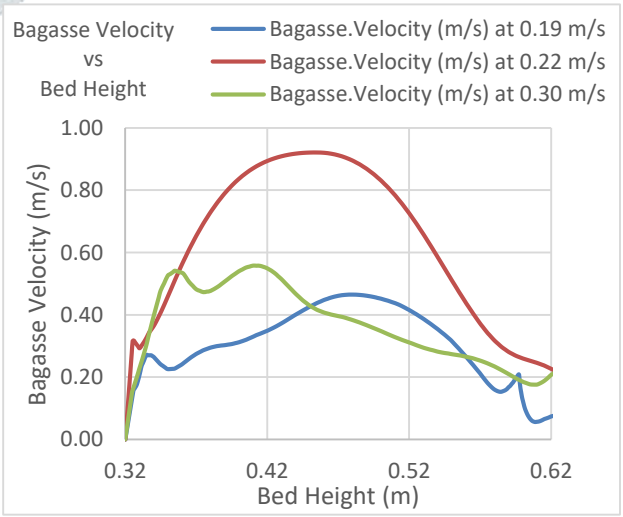

Fig 15. Graph of MSW velocity magnitude vs Bed Height at Different inlet Air Velocities

Fig 12 & 13 shows Volume fraction distribution of sugarcane bagasse in the reactor bed. Bagasse particles tend to be mostly located in the left and middle regions of the bed. Bagasse movement across the bed was predominantly upwards at the reactor's center-line and downwards in the near-wall region.Fig 14 and 15 shows velocity magnitude of bagasse at different air inlet

velocities. At velocities like 0.22 m/s solid particles velocity is increasing as the velocity increase solid particles of Bagasse going upward direction above distributor plate.

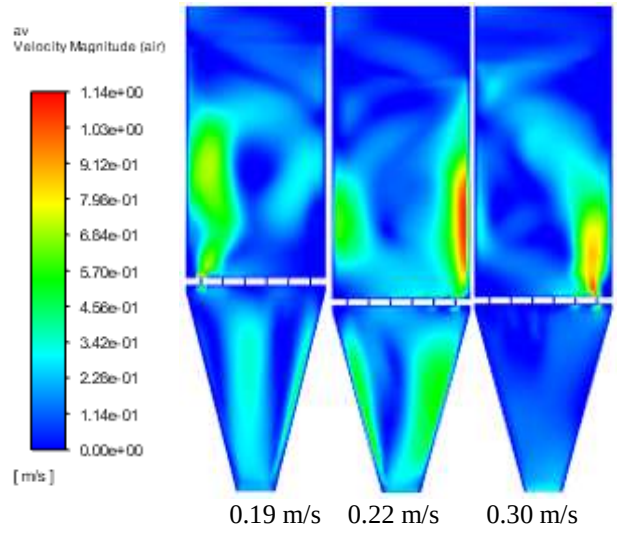

Fig 16. Air Velocity Magnitude at Different inlet Air Velocities

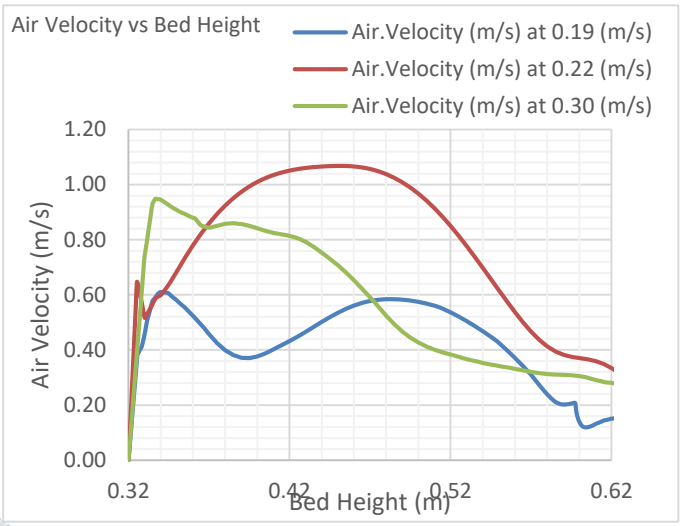

Fig 17. Graph of Air velocity magnitude vs Bed Height at Different air Inlet Velocities

Fig 16 and 17 shows air inlet velocities in bed height. As increase in velocity it shows various graph plots. At the end of bed height velocity increase between 0.19 to 0.35 m/s.

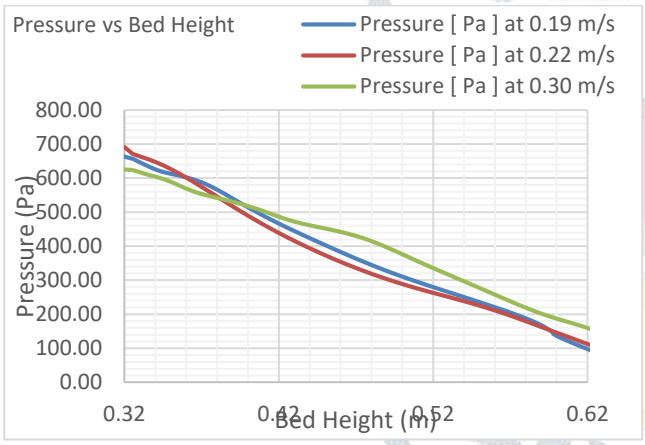

Fig 18. Pressure vs Bed Height at Different inlet Air Velocities

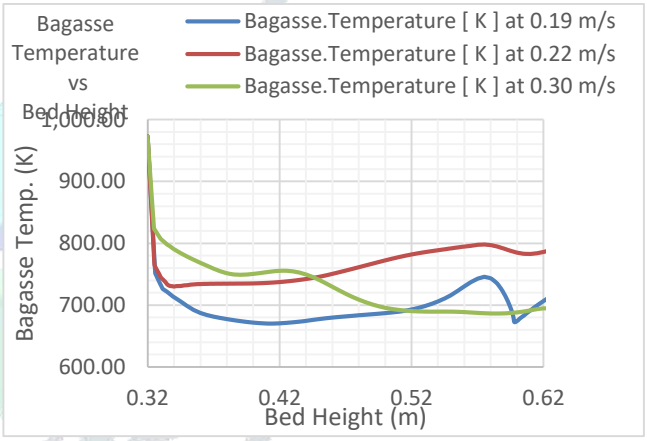

Fig 19. Bagasse Temperature vs Bed Height at Different inlet Air Velocities

Fig 18 shows pressure of air bagasse mixture in bed height. Starting pressure at different air inlet velocities was same. But at the end of bed height, it shows variation between 100 to 175 Pascal. Fig 19 shows Temperature distribution of bagasse particles Along the bed. It shows variation about 690 k to 780 k at different inlet velocities.

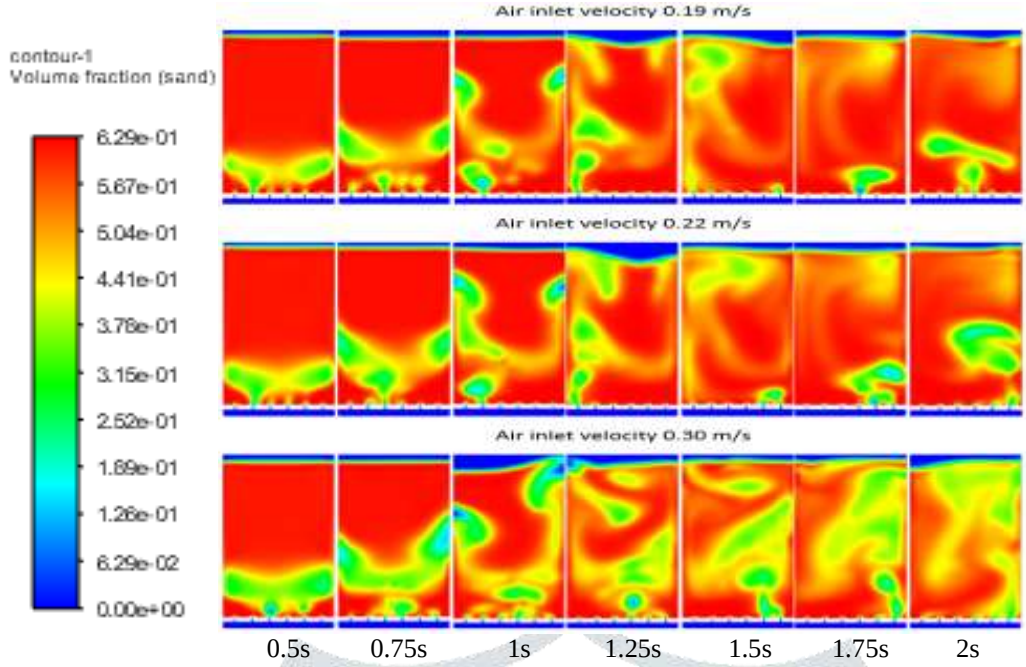

Fig 20. Volume fraction distribution for the Sand particles using the Syamlal and O'Brien drag model with three inlet velocities.

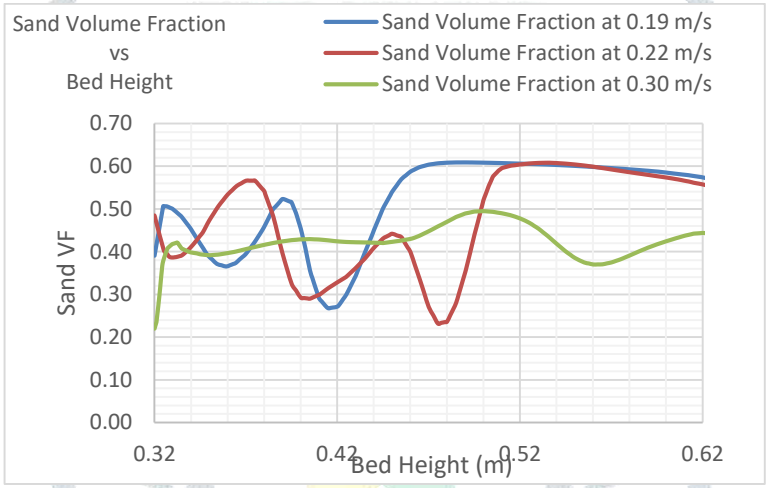

Fig 21. Graph of Sand volume fraction vs Bed Height at Different inlet Air Velocities

Fig 20 & 21 shows Volume fraction distribution of sand in the reactor bed. Sand particles were found to gather at the middle and bottom of the bed. This distribution showed a close correlation with the component's density and size of particles.

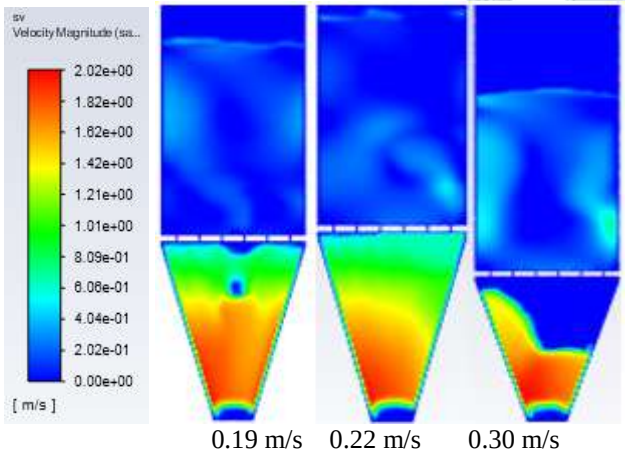

Fig 22. Sand Velocity Magnitude at Different air Inlet Velocities

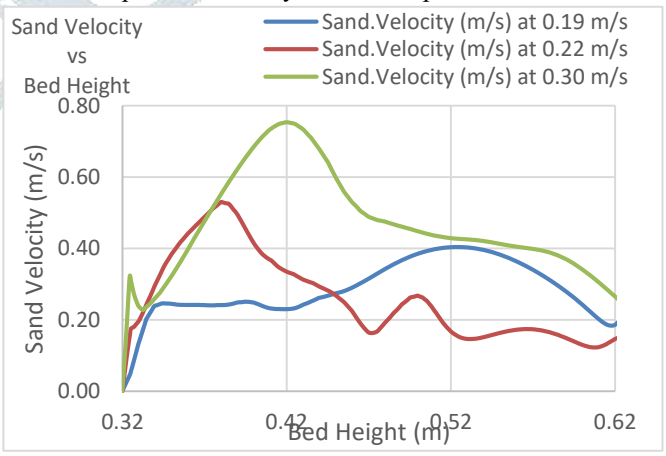

Fig 23. Graph of Sand velocity magnitude vs Bed Height at Different Inlet Air Velocities

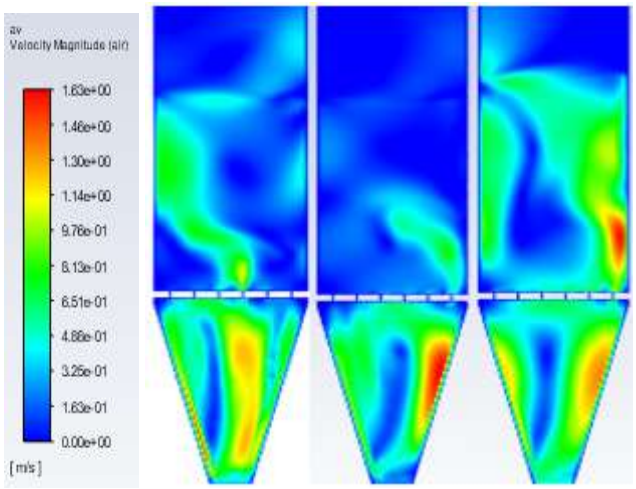

Fig 24. Air Velocity Magnitude at Different air Inlet Velocities

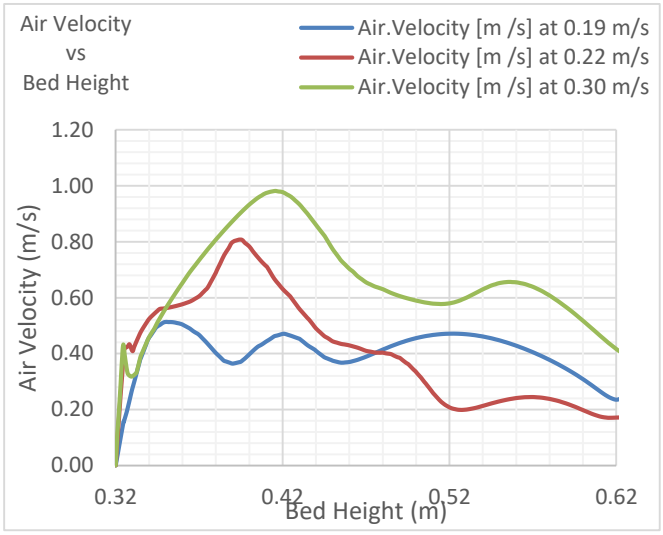

Fig 25. Graph of Air velocity magnitude vs Bed Height at Different inlet Air Velocities

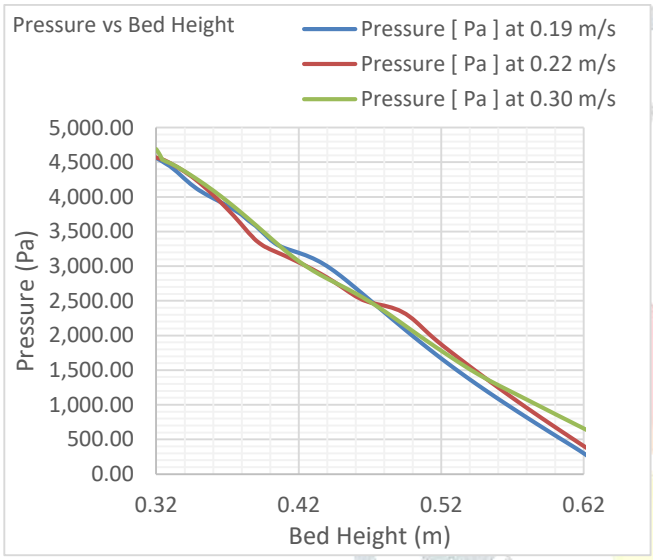

Fig 26. Graph of Pressure vs Bed Height at Different inlet Air Velocities

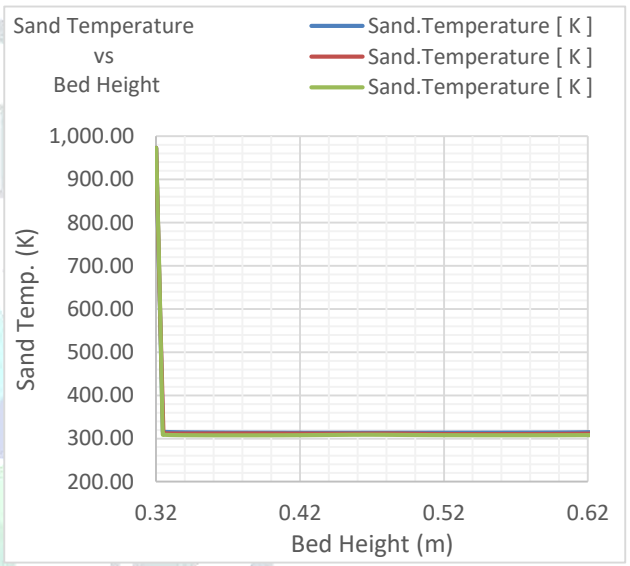

Fig 27. Sand Temperature vs Bed Height at Different Inlet Air Velocities

Fig 26 shows pressure of air sand mixture in bed height. Starting pressure at different air inlet velocities was same. But at the end of bed height, it shows variation between 300 to 650 Pascal. Fig 27 shows Temperature distribution of sand particles Along the bed. It shows no variation because its small thermal conductivity.

VIII. Conclusion

The model and simulation of the CFD 2D is done as an accurate illustration of a real Lab-scale bubbling fluidized bed to be built for future work. These results suggest that CFD simulations using the drag model of Syamlal and O'Brien are able to capture hydrodynamics in a gasifier in a BFBG, so the planned model provides a useful basis for additional activities in further CFD simulation of the fire component. BFBG structures have shown that MSW particles are most commonly found in the middle and upper bed regions. Sand particles were found to combine in the middle and under the bed. Bagasse particles tend to be mostly located in the left and middle regions of the bed. Bagasse movement across the bed was predominantly upwards at the reactor's center-line and downwards in the near-wall region. This distribution showed a close relationship with the size of the structure and the size of the particles. The light particles of MSW are separated at the top of the bed, and the heavy particles of MSW produce a better mixing character given its closest size to the sand. The small particles of MSW produced similar mixtures, due to their close proximity to sand particle size. Also, it was found that an increase in air velocity improved binary integration. The movement of the MSW across the bed was mainly upwards in the center of the reactor to the bottom of the region near the wall. The pressure across the bed height decreases due to sand and MSW particles in the air. No temperature differences occurred because the simulation time was only 2s. In the next study a BFBG lab scale model will be developed based on the design parameters and performance and compare the result with CFD data.

IX. References

[1]. Kunii, D., Levenspiel, O., & Levenspiel, O. (1990). Fluidized Reactor Models. 1. For Bubbling Beds of Fine, Intermediate, and Large Particles. 2. For the Lean Phase: Freeboard and Fast Fluidization. Industrial and Engineering Chemistry Research, 29(7), 1226–1234. https://doi.org/10.1021/ie00103a022

[2]. Ifin, N. E. (2001). Design and Construction of a. Congreso Sobre Traducción Automática, 8, 1–13. http://www.eamt.org/summitVIII/papers/bond.pdf

[3]. Souza-Santos, M. L. de. (2010). Solid Fuels Combustion and Gasification Modeling, Simulation, and Equipment Operations (2nd ed.). Taylor& Francis.
[4]. Wen-Ching Yang. (2003). Handbook of Fluidization and Fluid-Particle Systems. Marcel Dekker.
[5]. Rao, A., Curtis, J. S., Hancock, B. C., & Wassgren, C. (2010). The Effect of Column Diameter and Bed Height on Minimum Fluidization Velocity, 56(9). doi:10.1002/aic
[6]. Abd-Rabbo, M. A., Sakr, R. Y., Mohammad, M. A., & Mandour, M. M. (2019). CFD Simulation of Heat Transfer from Elliptic Tube Bundle Buried in a Bubbling Fluidized Bed. Asian Journal of Applied Chemistry Research, 4(3), 1–12. https://doi.org/10.9734/ajacr/2019/v4i330111
[7]. Li, J., & Yang, B. (2017). CFD simulation of bubbling fluidized beds using a local-structure-dependent drag model. Chemical Engineering Journal, 329, 100–115. https://doi.org/10.1016/j.cej.2017.05.164
[8]. Afrooz, I. E., Sinnathambi, C. M., Chuang, D. L., & Karuppanan, S. (2017). CFD simulation of bubbling fluidized bed: Effects of bed column geometry on hydrodynamics of gas-solid mixing. Materialwissenschaft Und Werkstofftechnik, 48(3–4), 226–234. https://doi.org/10.1002/mawe.201600761
[9]. Mertzis, D., Savvakis, S., & Samaras, Z. (n.d.). Cfd Simulation of a Bubbling Fluidized Bed Biomass Gasifier Using Ansa Meshing and Ansys Fluent.
[10]. Sharma, A., Wang, S., Pareek, V., Yang, H., & Zhang, D. (2014). CFD modeling of mixing/segregation behavior of biomass and biochar particles in a bubbling fluidized bed. Chemical Engineering Science, 106, 264–274. https://doi.org/10.1016/j.ces.2013.11.019